FRONTIERS OF PHYSICS

LETTER
Volume 19 / Issue 6 / 63208 / 2024

Temperature dependence of positive and negative magnetoresistances of tantalum-covered multiwalled carbon nanotubes

Julienne Impundu[1,2,*], Wenxiang Wang[1,2,*], Zheng Wei[1,2], Yushi Xu[1], Yu Wang[1], Jiawang You[1], Wenbin Huang[3,†], Yong Jun Li[1,2,‡], Lianfeng Sun[1,2,§]

1 CAS Key Laboratory of Nanosystem and Hierarchical Fabrication, Nanofabrication laboratory, CAS Center for Excellence in Nanoscience, National Center for Nanoscience and Technology, Beijing 100190, China
2 University of Chinese Academy of Sciences, Beijing 100049, China
3 Mechanical Engineering Research Institute, Xi'an 710032, China
*These two authors contributed equally to this work.
Corresponding authors. E-mail: †huangwenbinde-2008@163.com, ‡liyj@nanoctr.cn, §slf@nanoctr.cn
Received April 16, 2024; accepted June 17, 2024

ABSTRACT

Carbon nanotubes (CNTs) have garnered significant attention due to their remarkable electronic and magnetic properties. In this research, we introduced multiwalled carbon nanotubes covered with tantalum (MWNTs/Ta) to systematically modulate the magnetoresistive properties of the MWNTs/Ta hybrid nanostructures. We observed distinct changes in both positive and negative magnetoresistances of MWNTs/Ta across a broad temperature range using a physical property measurement system and a four-terminal method. This study on temperature-dependent magnetoresistive behavior of the MWNTs/Ta sheds light on the fundamental properties of carbon-based materials and holds promise for practical applications in the field of spintronic devices.

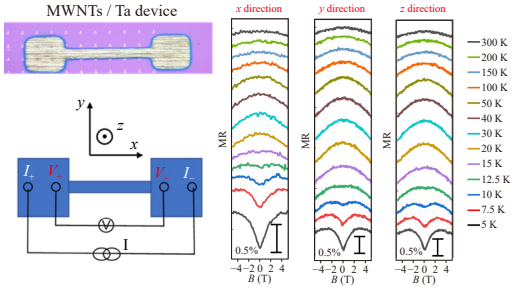

Keywords multiwalled carbon nanotubes, tantalum, magnetoresistance, temperature dependence, physical property measurement system, four-terminal method

1 Introduction

The remarkable electronic [1–5] and magnetic properties [6–11] of carbon nanotubes (CNTs) and nanomaterials [12, 13] have attracted great interest and attention. In recent years, extensive research has been dedicated to investigating the magnetic properties of CNTs and their possible application in spintronic devices, where control electron spin becomes critical [14–17]. A relatively weak spin–orbit coupling leads to a long spin relaxation time and spin diffusion length in CNTs [18–23]. Therefore, CNTs are ideal for spin regulation and transport. However, a giant challenge for the spintronic device of CNTs is to achieve the ferromagnetism/magnetic moment in CNTs, since carbon materials such as CNTs are commonly considered to be typical diamagnetic materials [24].

Magnetic impurities enclosed in the cavity and the adsorption of hydrogen atoms can induce magnetic moments in CNTs [25]. Another promising avenue involves the utilization of transition metals to induce magnetism in CNTs and manipulate their electrical behavior. Recently, an anomalous Hall effect in edge-bonded monolayer graphene demonstrated the ferromagnetism in graphene [26]. They chose molybdenum as the electrode due to the occurrence of a local solid–solid reaction during the process of magnetron sputtering. They showed that the anomalous Hall effect in pristine

Higher Education Press

https://doi.org/10.1007/s11467-024-1432-5

monolayer graphene provides indisputable evidence for the existence of a long-range ferromagnetic order. More recently, the first experimental realization of a four-terminal spin field effect transistor (FET) via a separate semiconducting single-walled carbon nanotube (SWNT) was reported [27]. Two partially open SWNT segments can be obtained when the Mo electrode is deposited using a magnetron sputtering.

Magnetoresistance (MR) is defined as the ability of a material to change the value of its electrical resistance in an externally applied magnetic field. The MR typically originated from charge inhomogeneity and other disorder in materials. The study of magnetoresistive behavior of metals can go back to experiments by L. Kelvin and E. Hall in 1857 and 1880, respectively. In 1928–1929, Kapitsa and Rutherford [28, 29] reported the magnetoresistive behavior of 37 materials. He observed large MR in bismuth, arsenic and graphite when the magnetic field reaches 30 T. MR exhibits parabolic in small fields and increases linearly in fields above several tesla. The common positive magnetoresistance occurs in metals. Anisotropic magnetoresistance (AMR) refers to the phenomenon that the resistivity of ferromagnetic materials changes with the angle between the magnetization and current direction. In addition, for ferromagnets, a characteristic butterfly loop will be observed when the magnetic field is changed for ferromagnetism in iron single crystals and ferromagnetic semiconductor (Ga, Mn)As [30, 31]. Therefore, magnetoresistance measurement is a direct and alternative method to detect and study magnetic order of Ta-MWNTs. Esquinazi and his colleagues [32] reported that highly oriented pyrolytic graphite (HOPG) samples exposed to irradiation show anisotropic AMR and negative MR with pronounced hysteresis loops, which demonstrated the ferromagnetism in HOPG after irradiated. Temperature is an important factor in the change of materials properties and also has a significant effect on the magnetoresistance of magnetic materials. As the temperature increases to the Curie temperature of ferromagnetic materials, long-range order is broken down. The Curie temperature of traditional dilute magnetic semiconductors and two-dimensional intrinsic ferromagnetic semiconductors are lower than room temperature [33, 34].

Ta is known for its paramagnetic nature, high melting point, excellent thermal stability and good electrical conductivity [35]. Its paramagnetic nature excludes the effect of electrode metal on the magnetoresistive signal of CNT. Wang *et al.* [36] showed that the sputtering process creates more defects on the surface of Ta-decorated CNTs. According to Lieb's theorem [37], these defective structures can induce magnetic moments in Ta-covered CNT [38, 39]. Temperature affects the magnitude and direction of the magnetic moment [40]. As the temperature increases, the magnetic moment decreases and the direction becomes more random, which can be reflected by the magnetoresistance behavior. Therefore, understanding the temperature-dependent behavior of magnetoresistance in MWNTs covered with Ta is essential for optimizing their performance in such applications.

In this study, we present our experimental procedures and describe the MWNTs/Ta device fabrication and magnetoresistance measurements performed under controlled temperatures using a Physical Property Measurement System (PPMS-ANC300) and four terminal techniques. We then elucidate the physical processes that contribute to magnetoresistance behavior by analyzing observed trends as a function of temperature. Our discussion focuses on positive and negative magnetoresistance separately and provides a comprehensive overview of how these phenomena evolve over a wide range of temperatures. This research has the potential to open up new avenues for the development of next-generation spintronic technologies with improved efficiency and functionality.

2 Experimental

The method used to fabricate the aligned MWNT films on a SiO_2/Si substrate was the spinning continuous yarns method [41–45] To ensure accurate test results, the MWNT film was soaked in a hydrochloric acid solution with a mass fraction of about 14.6% for 24 hours to eliminate the influence of ferromagnetic catalysts before device fabrication [Fig. 1(a)]. We then constructed MWNTs/Ta devices using hard templates and magnetron sputtering.

First, a metal mask is applied to the MWNT films. The metal mask has a dumbbell-shaped hollow in the middle, as shown in Fig. 1(b). The center hollow has a minimum size of 50 μm. Hard templates are directly used as a masking film to cover the sample to prevent the effect of residual glue on the performance of the device during exposure processes and allow several devices to be prepared at the same time. Second, magnetron sputtering (Lesker Lad 18) is used to deposit Ta metal onto MWNT films. The base pressure and power are about 1×10^{-5} torr and 400 W, respectively, with a deposition time of approximately 250 s. After removal of the metal mask [Fig. 1(c)], argon plasma etching [Fig. 1(d)] is used to remove the excess carbon nanotubes from outside the device. The device is then ready for electrical testing. The Ta metal electrode is sufficiently thick to protect the MWNT films. Therefore, only the external MWNTs to the device are eliminated and the structure of the device remains not changed. Optical images of MWNTs/Ta and pure Ta devices are shown in Fig. 2(a). The devices exhibit a dumbbell-shaped configuration with the MWNTs running parallel to the Ta metal bars. Due to electrode expansion during the process of deposition, the minimum size at the center of the final device is approximately 100 μm.

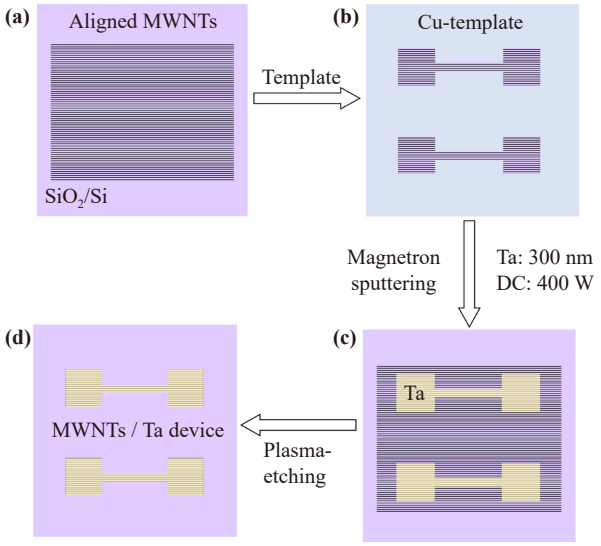

Fig. 1 Fabrication of aligned MWNTs covered with tantalum. **(a)** Aligned MWNTs grown on silicon wafers. **(b)** A metal mask with a dumbbell is positioned onto MWNTs. **(c)** The metal tantalum (Ta) is deposited onto the MWNTs using magnetron sputtering. **(d)** Optical images of MWNTs/Ta bar devices.

Using the same template and fabrication process, we also fabricated a pure Ta device. As shown in Fig. 2(b), the Ta thickness is ~305 nm.

The morphology of the MWNTs/Ta was characterized using an atomic force microscope (AFM Multimode 8HR, Bruker), as shown in Fig. 2(c). The average height of the thinned MWNTs along the white dashed line is ~142 nm, as shown in Fig. 2(d). This value is smaller than the tantalum metal electrode thickness (305 nm), indicating that the MWNTs are squeezed under the Ta metal electrode. Images of pristine MWNTs and MWNTs covered with Ta metal obtained via Hitachi scanning electron microscopy (SEM) (SU8220) [Figs. 2(e, f)]. The diameter of MWNTs after magnetron sputtering is significantly wider than that of the pristine MWNTs, indicating that MWNTs are well covered with Ta metal. The morphology is used to understand the surface area and orientation of the MWNTs, which affects the adhesion and coverage of the tantalum coating. We performed AFM characterization and SEM characterization of Ta-covered MWNTs. Through AFM characterization, we found that the thickness of the Ta metal film is greater than the height fluctuation of the MWNTs, indicating that the MWNTs are completely covered by Ta metal. Through SEM characterization, it was found that the morphology of the Ta-covered MWNTs was significantly different from that of the pristine MWNTs, and the diameter of the Ta-covered MWNTs seemed to increase significantly, indicating that Ta was perfectly covered on the MWNTs. Then we used EDX (SEM) to characterize the element distribution of Ta-covered MWNTs device. The distribution of carbon and Ta elements was observed in the EDX mapping [Figs. 2(g, h)]. However, the distribution of iron elements was not observed, which demonstrates that there are few ferromagnetic impurities in Ta-covered MWNTs. Subsequently, to execute low temperature test, the pure Ta and MWNTs/Ta devices are bonded to the PPMS holder [Fig. 3(a)]. A four-terminal method is utilized for resistance testing due to the elimination of contact resistance. Figure 3(b) depicts the schematic drawing of the four-terminal method in this work. The outer ends of the device act as I_+ and I_-,

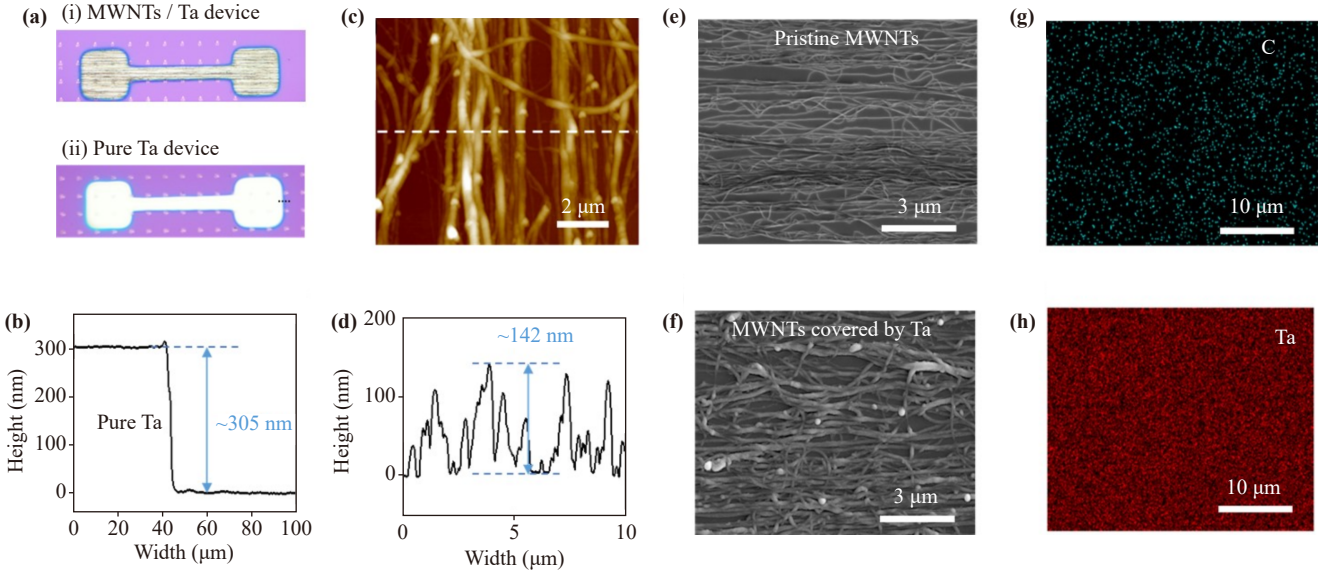

Fig. 2 Characterization of aligned MWNTs covered with Ta. **(a)** Optical images of (i) MWNTs/Ta device, (ii) pure Ta device, and **(b)** the height profile of Ta device. **(c)** AFM image of aligned MWNTs/Ta. **(d)** MWNTs/Ta height profile. **(e, f)** SEM image of pristine MWNTs and aligned MWNTs/Ta. **(g, h)** The elements distribution of Ta-covered MWNTs.

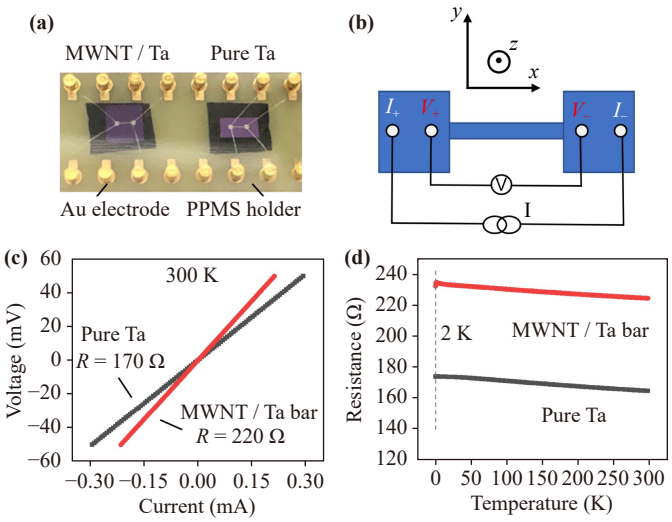

Fig. 3 Bar structures and transport properties of MWNTs/Ta and Ta bar devices. **(a)** Photograph of MWNTs/Ta bar (left) and Ta bar (right) devices. **(b)** The schematic drawing of the four-terminal method. **(c)** *I*–*V* characteristics of the devices in (a). **(d)** Resistance versus temperature of the devices in (a).

and the inner ends are used to measure the voltage difference $(V_+ - V_-)$. Finally, the resistance is obtained by Ohm's law. We conducted measurements of I_{ds} to achieve representative current–voltage (*I*–*V*) characteristic graphs of the Ta device and MWNTs/Ta device, which can be seen in Fig. 3(c). The device current varied linearly with voltage, and the resistance was 170 and 220 Ω for the Ta device and the MWNTs/Ta device, respectively. Figure 3(d) illustrates the variation in resistance as the temperature decreases from 300 to 2 K. The increase in resistances of the Ta device and Ta-covered MWNTs with decreasing temperature is mainly attributed to weak localization and electron–electron interactions in the Ta metal.

MR effect is a change in the material's resistance when exposed to an external magnetic field. We have carried out magnetoresistance tests on both pure Ta device and MWNTs/Ta device using the PPMS system. The transport performance of these devices in this work is measured in the temperature range of 5–300 K and scanning of magnetic fields from –5 to 5 T. We express the direction of the magnetic field out-of-plane, perpendicular to the substrate, which was denoted by *z*. The direction of the magnetic field in-plane, parallel to the aligned MWNTs, was denoted by *x*. Finally, the direction of the magnetic field, in-plane, perpendicular to the aligned MWNTs, was denoted by *y*. To investigate the influence of the magnetoresistance of the device at various temperatures and magnetic field directions during the test, the device resistance was measured continuously as a function of the magnetic field under electric current. Figure 4(a) shows the variation curves of the resistance of the MWNTs/Ta device and pure Ta device under magnetic field scanning in the *x* direction (–5 to 5 T). At 5 K, it can be seen that the resistance value of the MWNTs/Ta device gradually increases with increasing magnetic field strength and finally reaches the saturation value, and exhibits positive magnetoresistance. At 7.5 and 10 K, the resistance initially increases and then decreases as the magnetic field strength increases. As the temperature rises further (12.5 to 300 K), a negative magnetoresistive behavior occurs, which means the resistance decreases as the magnetic field strength increases. Therefore, in the MWNTs/Ta device, a transition from positive magnetoresistance to negative magnetoresistance is observed with increasing temperature, which shows "M" shaped magnetoresistance at around 7.5 K. This phenomenon has also been reported by Geim *et al.* [46]. For the screened graphene device, they observed the M-typing MR under a small magnetic field. As the temperature increases, the magnetoresistive behavior changes from "M" to positive magnetoresistive behavior, as shown in the red frame in the figure below. They attribute this M-shaped to Landau quantization and the electron-hole plasma. For Ta-covered MWNTs, as the temperature increases, the magnetoresistive behavior changes from positive magnetoresistive behavior to M-shaped to negative magnetoresistive behavior. However, the mechanism of temperature regulating the magnetoresistive behavior of Ta-covered MWNTs is not clear. In addition, the resistance of a pure Ta device has a positive magnetoresistance of 5 to 12.5 K. And it is independent of the magnetic field strength and maintains constant when temperature is higher than 12.5 K, which is significantly different from MWNTs/Ta device. This difference between the MWNTs/Ta device and the pure Ta device is mainly caused by the magnetic momentum of the partially unzipped MWNTs. The magnetic moment comes from the solid–solid chemical reaction between Ta and carbon atoms, which unzipped the SWNTs along the radial direction. Following the coating of MWNTs with Ta, the surface of MWNTs/Ta exhibited the formation of defect sites, which disrupted the regular arrangement of MWNT atoms. This resulted in alterations to the magnetic moments and an impact on the overall magnetic behavior, which is consistent with previous studies [47, 48]. When applying a magnetic field is applied in the *y* direction and *z* direction, similar behaviors are observed [Figs. 4(b) and (c)].

MR is defined as $MR = \frac{R(B)-R(0)}{R(0)}$, the device resistance under an external magnetic field B is denoted by $R(B)$, while $R(0)$ represents the device resistance in the absence of an external magnetic field. As shown in Fig. 5, the variation trend of MR (MWNTs/Ta device) with temperature is summarized. At 5 K, the MR of the MWNTs/Ta device exhibits a positive magnetoresistance under 5 T in the *x*, *y*, and *z* directions. The values of MR are about 0.3‰, 0.36‰, and 0.34‰, respectively.

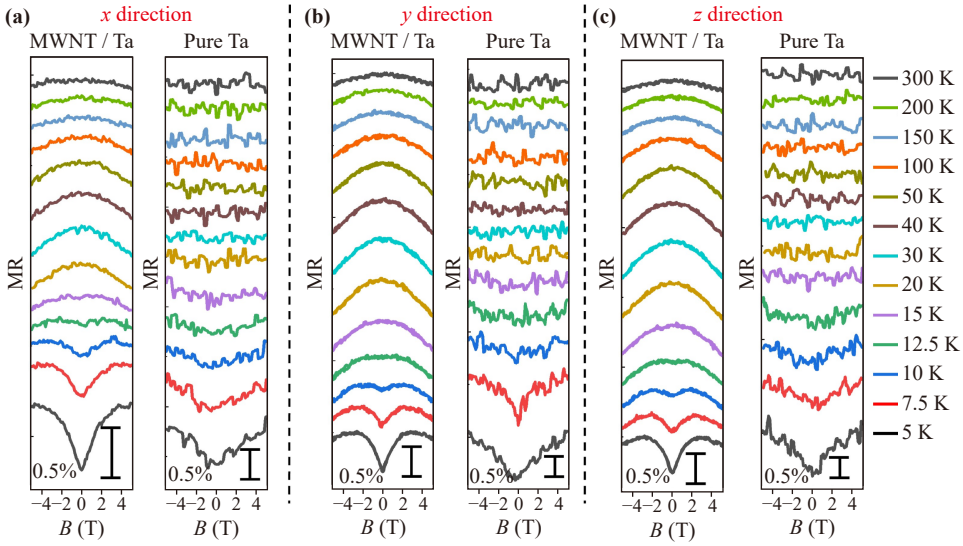

Fig. 4 Magnetotransport properties for the MWNTs/Ta bar device and the pure Ta bar device were examined as a function of temperature in: **(a)** x direction, **(b)** y direction, and **(c)** z direction.

As the temperature increases, negative magnetoresistive behavior is observed and reaches a maximum of 15 K. With further increase in temperature, the negative magnetoresistive behavior slowly weakens and approaches zero.

Here, the negative magnetoresistance in the device made of aligned MWNTs covered with Ta is not due to the variation of magnetoresistance in Ta metal but due to other reasons. Chiral anomalies, the effect of ferromagnetic impurities and the magnetic moments at the edges of the MWNTs may be responsible for the influence of negative magnetoresistance of MWNTs/Ta devices at 10–300 K. First, Chiral anomalies in which electronic states of a particular chirality are not preserved when exposed to parallel magnetic and electric fields, are a common feature of negative magnetoresistance in materials and are usually found in highly conductive materials such as Weyl semimetals [49–52]. The magnetic field along the direction of the electric field is quite weak when the external magnetic field is parallel to the electric field. The chiral anomaly system exhibits a rapid decrease in resistance with an increasing magnetic field, resulting in a negative magnetoresistance phenomenon. The negative magnetoresistance phenomenon observed in our experiments was not attributed to chiral anomalies. This phenomenon was observed regardless of the direction of the external magnetic field relative to the electric field. Second, the preparation of MWNTs by chemical vapor deposition requires the use of ferromagnetic catalysts. It cannot be excluded that the MWNTs used in our experiment contain trace amounts of ferromagnetic impurities, although subsequent transfer treatments were performed. Before device fabrication, we soaked silicon wafers with MWNTs in a solution of hydrochloric acid for 24 hours. The EDX mapping in Figs. 2(g) and (h) demonstrates that there are no ferromagnetic impurities in Ta-covered MWNTs. Based on the above discussion, it is suggested that the effect of negative magnetoresistance in the Ta-covered MWNTs device may be due to the magnetic moments at the open ends of the MWNTs. This is supported by experimental evidence of the magnetic moment and ferromagnetism of radial open-

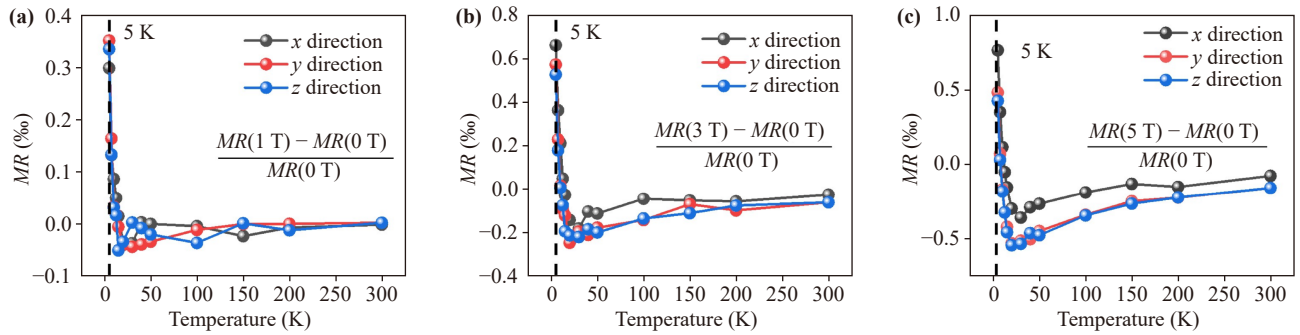

Fig. 5 Magnetoresistance (MR) behavior at different temperatures along different magnetic field directions: **(a)** x axis, **(b)** y axis, and **(c)** z axis of MWNTs/Ta bar device.

ended CNTs, which were applied to CNT spin devices and CNT film spin transistors [53].

3 Conclusion

We constructed MWNTs/Ta devices and pure Ta devices using template methods and magnetron sputtering. The device made from MWNTs/Ta had positive magnetoresistance at 5 K. Between 5 and 12.5 K, its magnetoresistance shifted from positive to negative and it displayed "M"-shaped behavior. In contrast to the test results for pure Ta devices, it demonstrated negative magnetoresistance between 12.5 and 300 K. The high-energy Ta atoms produced during magnetron sputtering reacted with MWNTs, resulting in magnetic moments at the radial opening of MWNTs, which made the MWNTs/Ta device less resistant to magnetoresistance. This work demonstrates the existence of magnetic moments at the radial openings of MWNTs and offers new perspectives on the ferromagnetism of carbon-based nanomaterials.

Declarations The authors declare that they have no competing interests and there are no conflicts.

Acknowledgements J. Impundu gratefully acknowledges the financial support provided by the Organization for Women in Science for the Developing World (OWSD) Postgraduate Fellowship Program and the Swedish International Development Cooperation Agency (SIDA), the National Natural Science Foundation of China (No. 52372256), the CAS Project for Young Scientists in Basic Research (YSBR-030), the Major Nanoprojects of Ministry of Science and Technology of China (Grant No. 2018YFA0208403), and the Strategic Priority Research Program of Chinese Academy of Sciences (Grant No. XDB36000000).

References

1. T. W. Odom, J. L. Huang, P. Kim, and C. M. Lieber, Structure and electronic properties of carbon nanotubes, *J. Phys. Chem. B* 104(13), 2794 (2000)
2. T. W. Ebbesen, H. J. Lezec, H. Hiura, J. W. Bennett, H. F. Ghaemi, and T. Thio, Electrical conductivity of individual carbon nanotubes, *Nature* 382(6586), 54 (1996)
3. M. R. Falvo, G. J. Clary, V. II Taylor, F. P. Jr Chi, S. Jr Brooks, S. Washburn, and R. Superfine, Bending and buckling of carbon nanotubes under large strain, *Nature* 389(6651), 582 (1997)
4. P. Avouris, M. Freitag, and V. Perebeinos, Carbon-nanotube photonics and optoelectronics, *Nat. Photonics* 2(6), 341 (2008)
5. P. Avouris and R. Martel, Progress in carbon nanotube electronics and photonics, *MRS Bull.* 35(4), 306 (2010)
6. F. Kuemmeth, S. Ilani, D. C. Ralph, and P. L. McEuen, Coupling of spin and orbital motion of electrons in carbon nanotubes, *Nature* 452(7186), 448 (2008)
7. J. Guo, H. Jiang, Y. Teng, Y. Xiong, Z. Chen, L. You, and D. Xiao, Recent advances in magnetic carbon nanotubes: Synthesis, challenges and highlighted applications, *J. Mater. Chem. B* 9(44), 9076 (2021)
8. W. Wang, J. Impundu, J. Jin, Z. Peng, H. Liu, Z. Wei, Y. Xu, Y. Wang, J. You, W. Fan, Y. J. Li, and L. Sun, Ferromagnetism in sp^2 carbon, *Nano Res.* 16, 12883 (2023)
9. Z. Li, S. Li, Y. Xu, and N. Tang, Recent advances in magnetism of graphene from 0D to 2D, *Chem. Commun. (Camb.)* 59(42), 6286 (2023)
10. K. F. Mak, J. Shan, and D. C. Ralph, Probing and controlling magnetic states in 2D layered magnetic materials, *Nat. Rev. Phys.* 1(11), 646 (2019)
11. J. Impundu, S. Hussain, E. Minani, H. Liu, Y. J. Li, and L. Sun, Local magnetic characterization of 1D and 2D carbon nanomaterials with magnetic force microscopy techniques: A review, *Mater. Today Commun.* 35, 106103 (2023)
12. Z. Chen, J. Li, T. Li, T. Fan, C. Meng, C. Li, J. Kang, L. Chai, Y. Hao, Y. Tang, O. A. Al-Hartomy, S. Wageh, A. G. Al-Sehemi, Z. Luo, J. Yu, Y. Shao, D. Li, S. Feng, W. J. Liu, Y. He, X. Ma, Z. Xie, and H. Zhang, A CRISPR/Cas12a-empowered surface plasmon resonance platform for rapid and specific diagnosis of the Omicron variant of SARS-CoV-2, *Natl. Sci. Rev.* 9(8), nwac104 (2022)
13. F. Zheng, Z. Chen, J. Li, R. Wu, B. Zhang, G. Nie, Z. Xie, and H. Zhang, A highly sensitive CRISPR-empowered surface plasmon resonance sensor for diagnosis of inherited diseases with femtomolar-level real-time quantification, *Adv. Sci. (Weinh.)* 9(14), 2105231 (2022)
14. Y. Gu, Z. Qiu, and K. Müllen, Nanographenes and graphene nanoribbons as multitalents of present and future materials science, *J. Am. Chem. Soc.* 144(26), 11499 (2022)
15. Y. Liu, C. Zeng, J. Zhong, J. Ding, Z. M. Wang, and Z. Liu, Spintronics in two-dimensional materials, *Nano-Micro Lett.* 12(1), 93 (2020)
16. E. C. Ahn, 2D materials for spintronic devices, *npj 2D Mater. Appl.* 4(1), 17 (2020)
17. P. Ghising, C. Biswas, and Y. H. Lee, Graphene spin valves for spin logic devices, *Adv. Mater.* 35(23), 2209137 (2023)
18. E. A. Laird, F. Kuemmeth, G. A. Steele, K. Grove-Rasmussen, J. Nygård, K. Flensberg, and L. P. Kouwenhoven, Quantum transport in carbon nanotubes, *Rev. Mod. Phys.* 87(3), 703 (2015)
19. W. D. Rice, R. T. Weber, P. Nikolaev, S. Arepalli, V. Berka, A. L. Tsai, and J. Kono, Spin relaxation times of single-wall carbon nanotubes, *Phys. Rev. B* 88(4), 041401 (2011)
20. B. G. Márkus, M. Gmitra, B. Dóra, G. Csősz, T. Fehér, P. Szirmai, B. Náfrádi, V. Zólyomi, L. Forró, J. Fabian, and F. Simon, Ultralong 100 ns spin relaxation time in graphite at room temperature, *Nat. Commun.* 14(1), 2831 (2023)
21. H. Idzuchi, M. B. Martin, Y. Otani, B. Dlubak, P. Seneor, A. Anane, H. Jaffres, and A. Fert, Handbook of Spintronics, Dordrecht, Springer, 2015
22. X. Gu, L. Guo, Y. Qin, T. Yang, K. Meng, S. Hu, and X. Sun, Challenges and prospects of molecular spintron-

ics, *Precis. Chem.* 2(1), 1 (2024)
23. Y. Liu, C. Zeng, J. Zhong, J. Ding, Z. M. Wang, and Z. Liu, Spintronics in two-dimensional materials, *Nano-Micro Lett.* 12(1), 93 (2020)
24. J. W. McClure, Diamagnetism of graphite, *Phys. Rev.* 104(3), 666 (1956)
25. E. C. Lee, Y. S. Kim, Y. G. Jin, and K. J. Chang, First-principles study of hydrogen adsorption on carbon nanotube surfaces, *Phys. Rev. B* 66(7), 073415 (2002)
26. H. Liu, H. Wang, Z. Peng, J. Jin, Z. Wang, K. Peng, W. Wang, Y. Xu, Y. Wang, Z. Wei, D. Zhang, Y. J. Li, W. Chu, and L. Sun, An anomalous Hall effect in edge-bonded monolayer graphene, *Nanoscale Horiz.* 8(9), 1235 (2023)
27. J. Liu, Z. Peng, J. Cai, J. Yue, H. Wei, J. Impundu, H. Liu, J. Jin, Z. Yang, W. Chu, Y. J. Li, G. Wang, and L. Sun, A room-temperature four-terminal spin field effect transistor, *Nano Today* 38, 101138 (2021)
28. P. Kapitza and E. Rutherford, The study of the specific resistance of bismuth crystals and its change in strong magnetic fields and some allied problems, *Proc. R. Soc. Lond. A* 119(782), 358 (1928)
29. P. Kapitza, The change of electrical conductivity in strong magnetic fields (Part II): The analysis and the interpretation of the experimental results, *Proc. R. Soc. Lond.* 123, 292 (1929)
30. R. V. Coleman and A. Isin, Magnetoresistance in iron single crystals, *J. Appl. Phys.* 37(3), 1028 (1966)
31. Y. Li, Y. F. Cao, G. N. Wei, Y. Li, Y. Ji, K. Y. Wang, K. W. Edmonds, R. P. Campion, A. W. Rush-forth, C. T. Foxon, and B. L. Gallagher, Anisotropic current-controlled magnetization reversal in the ferromagnetic semiconductor (Ga, Mn)As, *Appl. Phys. Lett.* 103(2), 022401 (2013)
32. P. Esquinazi, J. Barzola-Quiquia, D. Spemann, M. Rothermel, H. Ohldag, N. García, A. Setzer, and T. Butz, Magnetic order in graphite: Experimental evidence, intrinsic and extrinsic difficulties, *J. Magn. Magn. Mater.* 322(9–12), 1156 (2010)
33. L. Chen, X. Yang, F. Yang, J. Zhao, J. Misuraca, P. Xiong, and S. von Molnár, Enhancing the Curie temperature of ferromagnetic semiconductor (Ga, Mn)As to 200 K via nanostructure engineering, *Nano Lett.* 11(7), 2584 (2011)
34. X. Li, J. W. Li, J. Y. You, G. Su, and B. Gu, High Curie temperature and high hole mobility in diluted magnetic semiconductors (B, Mn)X (X = N, P, As, Sb), cond-mat/2311.11283 (2023)
35. L. Malter and D. B. Langmuir, Resistance, emissivities and melting point of tantalum, *Phys. Rev.* 55(8), 743 (1939)
36. Z. Wang, Y. Zuo, Y. Li, X. Han, X. Guo, J. Wang, B. Cao, L. Xi, and D. Xue, Improved field emission properties of carbon nanotubes decorated with Ta layer, *Carbon* 73, 114 (2014)
37. O. V. Yazyev and L. Helm, Defect-induced magnetism in graphene, *Phys. Rev. B* 75(12), 125408 (2007)
38. G. Wang, M. J. Chen, F. Yu, L. J. Xue, Y. Deng, J. Zhang, X. Y. Qi, Y. Gao, W. G. Chu, G. T. Liu, H. F. Yang, C. Z. Gu, and L. F. Sun, Giant magnetic moment at open ends of multiwalled carbon nanotubes, *Chin. Phys. B* 24(1), 016202 (2015)
39. J. Zhang, Y. Deng, T. T. Hao, X. Hu, Y. Y. Liu, Z. S. Peng, J. P. Nshimiyimana, X. N. Chi, P. Wu, S. Y. Liu, Z. Zhang, J. J. Li, G. T. Wang, W. G. Chu, C. Z. Gu, and L. F. Sun, Large magnetic moment at sheared ends of single-walled carbon nanotubes, *Chin. Phys. B* 27(12), 128101 (2018)
40. W. Z. Zhuo, B. Lei, S. Wu, F. H. Yu, C. S. Zhu, J. H. Cui, Z. L. Sun, D. H. Ma, M. Z. Shi, H. H. Wang, W. X. Wang, T. Wu, J. J. Ying, S. W. Wu, Z. Y. Wang, and X. H. Chen, Manipulating ferromagnetism in few-layered $Cr_2Ge_2Te_6$, *Adv. Mater.* 33(31), 2008586 (2021)
41. K. L. Jiang, Q. Li, and S. Fan, Spinning continuous carbon nanotube yarns, *Nature* 419(6909), 801 (2002)
42. M. Zhang, K. R. Atkinson, and R. H. Baughman, Multifunctional carbon nanotube yarns by downsizing an ancient technology, *Science* 306(5700), 1358 (2004)
43. X. Lepró, M. D. Lima, and R. H. Baughman, Spinnable carbon nanotube forests grown on thin, flexible metallic substrates, *Carbon* 48(12), 3621 (2010)
44. S. Zhang, L. Zhu, M. L. Minus, H. G. Chae, S. Jagannathan, C. P. Wong, J. Kowalik, L. B. Roberson, and S. Kumar, Solid-state spun fibers and yarns from 1-mm long carbon nanotube forests synthesized by water-assisted chemical vapor deposition, *J. Mater. Sci.* 43(13), 4356 (2008)
45. C. D. Tran, W. Humphries, S. M. Smith, C. Huynh, and S. Lucas, Improving the tensile strength of carbon nanotube spun yarns using a modified spinning process, *Carbon* 47(11), 2662 (2009)
46. N. Xin, J. Lourembam, P. Kumaravadivel, A. E. Kazantsev, Z. Wu, C. Mullan, J. Barrier, A. A. Geim, I. V. Grigorieva, A. Mishchenko, A. Principi, V. I. Fal'ko, L. A. Ponomarenko, A. K. Geim, and A. I. Berdyugin, Giant magnetoresistance of Dirac plasma in high-mobility graphene, *Nature* 616(7956), 270 (2023)
47. S. S. Alexandre, M. S. C. Mazzoni, and H. Chacham, Edge states and magnetism in carbon nanotubes with line defects, *Phys. Rev. Lett.* 100(14), 146801 (2008)
48. M. E. Khan, Q. Wali, M. Aamir, and Y. H. Kim, Spin transport properties of carbon nanotubes by ferromagnetic zigzag triangular defects: A first-principles study, *Mater. Today Commun.* 32, 104074 (2022)
49. C. Zhang, E. Zhang, W. Wang, Y. Liu, Z. G. Chen, S. Lu, S. Liang, J. Cao, X. Yuan, L. Tang, Q. Li, C. Zhou, T. Gu, Y. Wu, J. Zou, and F. Xiu, Room-temperature chiral charge pumping in Dirac semimetals, *Nat. Commun.* 8(1), 13741 (2017)
50. Q. Li, D. E. Kharzeev, C. Zhang, Y. Huang, I. Pletikosić, A. V. Fedorov, R. D. Zhong, J. A. Schneeloch, G. D. Gu, and T. Valla, Chiral magnetic effect in $ZrTe_5$, *Nat. Phys.* 12(6), 550 (2016)
51. N. Ong and S. Liang, Experimental signatures of the chiral anomaly in Dirac–Weyl semimetals, *Nat. Rev. Phys.* 3(6), 394 (2021)
52. X. Huang, L. Zhao, Y. Long, P. Wang, D. Chen, Z. Yang, H. Liang, M. Xue, H. Weng, Z. Fang, X. Dai, and G. Chen, Observation of the chiral-anomaly-induced negative magnetoresistance in 3D Weyl semimetal TaAs, *Phys. Rev. X* 5(3), 031023 (2015)
53. J. Wu and F. Hagelberg, Magnetism in finite-sized single-walled carbon nanotubes of the zigzag type, *Phys. Rev. B* 79(11), 115436 (2009)